sustainability

MDPI

Article

Urban Flood Risk Sustainable Management: Risk Analysis of Dam Break Induced Flash Floods in Mountainous Valley Cities

Yuanyuan Liu [1,2], Yesen Liu [1,2,*], Qian Yu [1,2] and Shu Liu [1]

[1] State Key Laboratory of Water Cycle and Water Security, China Institute of Water Resources and Hydropower Research, Beijing 100038, China; liuyy@iwhr.com (Y.L.); yuqian@iwhr.com (Q.Y.)
[2] Key Laboratory of River Basin Digital Twinning of Ministry of Water Resources, Beijing 100038, China
* Correspondence: liuys@iwhr.com

Abstract

Small reservoirs in hilly areas serve as critical water conservancy infrastructure, playing an essential role in flood control, irrigation, and regional water security. However, dam-break events pose significant risks to downstream urban areas, threatening the sustainability and resilience of cities. This study takes Guangyuan City as a case study and employs numerical simulation methods—including dam-break modeling, hydrological modeling, and hydrodynamic modeling—to analyze the impact of dam-break floods on downstream urban regions. The results reveal that dam failure in small reservoirs can cause peak flood velocities exceeding 15 m/s, severely endangering urban infrastructure, ecosystems, and public safety. Additionally, for reservoirs with large catchment areas, dam-break floods combined with rainfall-induced flash floods may create compound disaster effects, intensifying urban flood risks. These findings underscore the importance of sustainable reservoir management and integrated flood risk strategies to enhance urban resilience and reduce disaster vulnerability. This research contributes to sustainable development by providing scientific insights and practical support for flood risk mitigation and resilient infrastructure planning in mountainous regions.

Keywords: mountainous city; integrated flood and waterlogging management; dam-break flood; flash flood risk; small reservoir; sustainable management

check for updates

Academic Editor: Faccini Francesco

Received: 20 May 2025
Revised: 12 June 2025
Accepted: 18 June 2025
Published: 25 June 2025

Citation: Liu, Y.; Liu, Y.; Yu, Q.; Liu, S. Urban Flood Risk Sustainable Management: Risk Analysis of Dam Break Induced Flash Floods in Mountainous Valley Cities. *Sustainability* **2025**, *17*, 5863. https://doi.org/10.3390/su17135863

Copyright: © 2025 by the authors. Licensee MDPI, Basel, Switzerland. This article is an open access article distributed under the terms and conditions of the Creative Commons Attribution (CC BY) license (https://creativecommons.org/licenses/by/4.0/).

1. Introduction

Mountain and river valley cities are cities located in mountainous and hilly areas, with built-up areas or core parts located in river valleys [1]. Generally, the mountain valley cities upstream of the mountainous areas have a limited distribution of reservoirs. They play an important role in flood control, irrigation and other aspects, but place a certain amount of pressure on downstream cities in terms of flood control. In the event of dam failure, there may be serious impacts on downstream cities [2]. According to statistics, small reservoirs accounted for more than 90% of the dam failures that occurred from 1991 to 2013. In recent years, as the global climate has changed, the frequency and intensity of short-duration heavy rainfall have increased year after year [3,4]. If rainfall produces excessive flooding that exceeds the discharge capacity of the reservoir, it is susceptible to dam failure. The superimposition of dam failure floods and flash floods formed by heavy rainfall poses a great threat to the lives and properties of the people, and urban flood risk management faces serious challenges [5]. With the development of mountainous urban economies, urban sprawl and high population and economic concentration, the impact of

dam-busting flash floods has become increasingly serious [6,7]; how to effectively improve the flood control capacity of mountain cities is the main problem that needs to be solved at present [8].

General measures to enhance urban flood control mainly involve constructing higher-standard flood control projects and expanding the scope of flood protection zones, which have played a significant role in improving regional flood control capabilities. In recent years, with the frequent occurrence of extreme rainfall events, engineering measures alone have struggled to address the flooding disasters caused by such extreme events. Particularly in mountain flood disaster prevention, a combination of engineering and non-engineering measures can be adopted, achieved by establishing a comprehensive mountain flood early warning system and emergency response framework [9]. Among these, mountain flood dam breach risk analysis is a critical component. By developing dam breach models, hydrological models, and hydrodynamic models, it is possible to conduct detailed simulations and predictions of mountain floods and dam breach risks triggered by heavy rainfall in hilly areas. This enables risk pre-simulation, allowing for early forecasting and warnings before heavy rain arrives, providing residents with sufficient evacuation time, and maximally ensuring the safety of people's lives and property.

Scholars have conducted in-depth studies on flash floods as well as dam failure flood risk assessment from different perspectives and have achieved fruitful results. Reed [10] developed a mountain flood forecasting system based on distributed hydrological models. Elbastawesy [11] utilizes remote sensing and geographic information systems to model flash floods in the Wadi Hudain watershed of Egypt. Santos [12] conducted a risk analysis of flash floods in the Douro River Basin (northeastern Portugal) based on geographic information systems. Dutta [13] analyzing and evaluating the risk of flash flood inundation by establishing one- and two-dimensional hydrodynamic coupled numerical simulation models of flooding evolution in flash flood gullies. Vladimir [14] analyzes the causes and environmental impacts of the collapse of the Karamkenkin Tailing Dam in the Russian Far East through a model. Youssef [15] estimation of flash flood risk along St. Catherine's Road in the southern Sinai Peninsula, Egypt, using GIS morphometry and satellite imagery. Ballesteros [16] analyzed the characteristics of flash floods in four small watersheds in mountainous areas without data using the tree ring analysis method.

Mountain cities, due to their unique topography and hydrological characteristics, have seen flood control research focus on hydrodynamic modeling, nature-based solutions, and urban resilience planning. With the economic development of mountain cities, integrating dam break flood risk with mountain city flood control to propose comprehensive solutions for multiple disaster risks has become a research hotspot.

Cai [17] utilized Computational Fluid Dynamics (CFD) models to simulate the dynamic characteristics of various attributes of flood-affected entities in three-dimensional complex urban environments. Kritikos [18] developed a geographic information system (GIS)-based approach for shallow landslide/debris-flow susceptibility assessment, application to western Southern Alps of New Zealand. He [19] proposes a method of estimating the inundation area in urban mountainous zones based on the soil conservation service curve number (SCS-CN) model. Ouyang [20] proposed a two-dimensional mountainous mass flow dynamic procedure solver (Massflow-2D) using the MacCormack-TVD finite difference scheme. This model was applied to the landslide in Hong Kong in 1993 and the Nora debris flow in the Italian Alps in 2000. These research results on the simulation and analysis of dam failures caused by flash floods have played a major role in the forecasting and early warning of flash floods.

This study takes Guangyuan City, Sichuan Province, China, as a case study. It constructs dam breach models, hydrological models, and one- and two-dimensional coupled

hydrodynamic models for the upstream reservoir, the small watershed downstream of the dam, and the main urban area downstream. These models simulate the impact of mountain floods in the downstream watershed, with and without dam breaches in the upstream small reservoir, on the downstream urban area. The aim is to provide technical support for flood prevention and drainage risk management in mountainous valley cities.

2. Research Process and Methods

2.1. Research Process

Guangyuan City is located in northern Sichuan Province, China, situated in the transitional zone between mountainous terrain and the Sichuan Basin. The central urban area is traversed by multiple rivers, including the Jialing River, Bailong River, Qingjiang River, Nan River, and Changtan River, making it a typical mountain valley city. The upstream hilly area 11 has small reservoirs, as shown in Figure 1. In the event of a dam breach combined with heavy rainfall, these reservoirs pose significant risks to the downstream urban area.

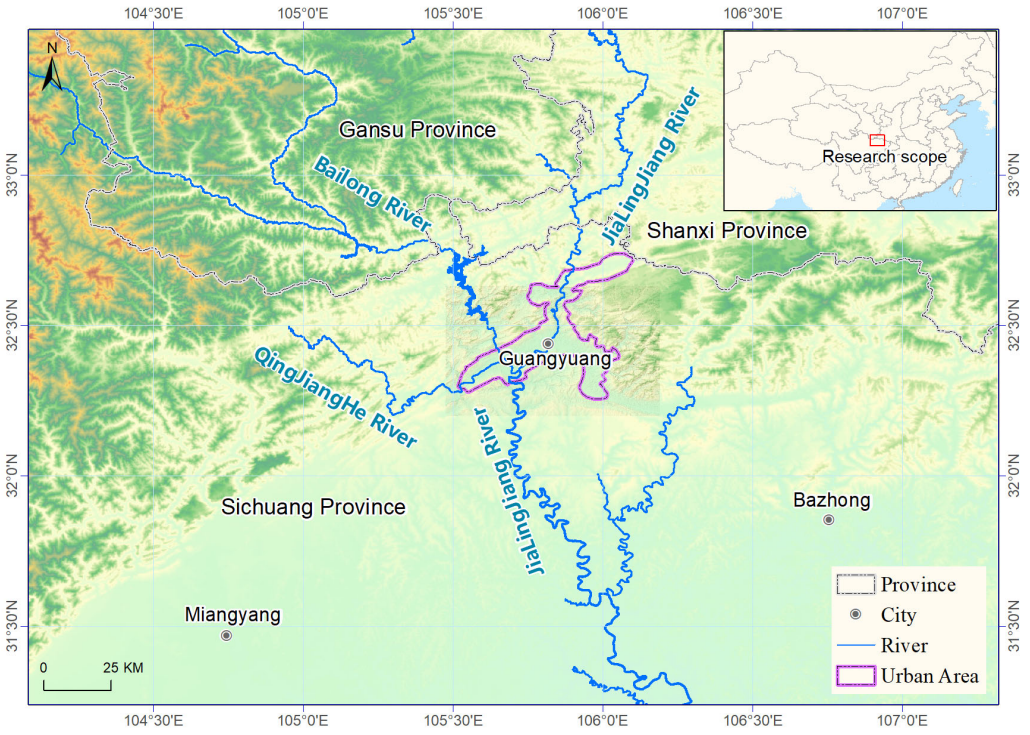


Figure 1. Research scope map.

Based on the topographic characteristics, river distribution, and engineering infrastructure of Guangyuan City, this study develops dam breach models, hydrological models, and coupled hydrological–hydrodynamic models to simulate and analyze potential dam breach and mountain flood risks in the central urban area. Specifically, a dam breach model is constructed to simulate reservoir flood discharge during a breach; a distributed hydrological model is developed to simulate the runoff generation and confluence processes in the downstream area under different rainfall recurrence intervals; and a hydrodynamic model is established to simulate the impact of superimposed dam breach floods and mountain floods on the urban area. The technical framework is illustrated in Figure 2.

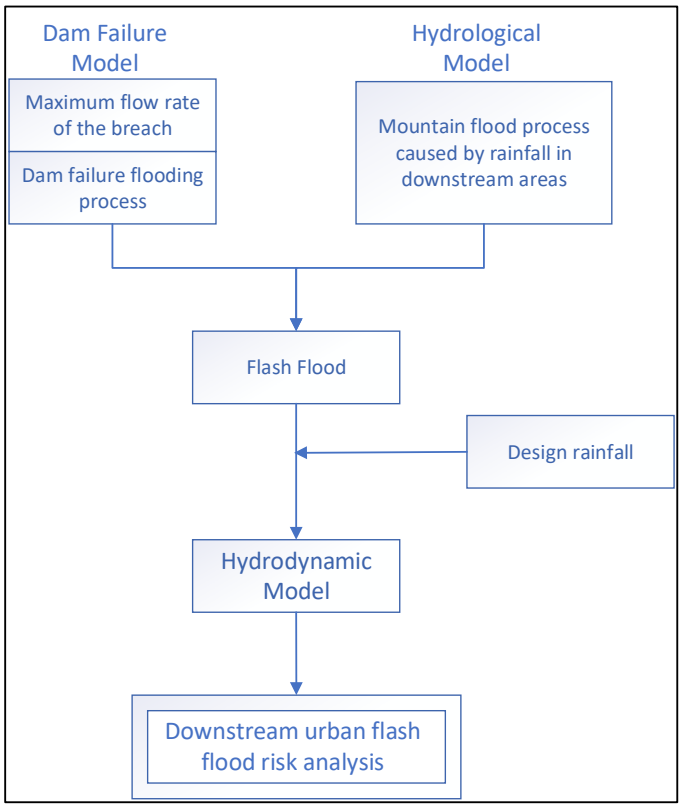


Figure 2. Research flow chart.

2.2. Scope of the Study

Since there is no exchange of water between sub watersheds in the Hill District, individual reservoirs only impact the sub watersheds in which they are located, while other sub watersheds do not exchange water. Therefore, combined with the topographic characteristics of the subsurface and the division of the sub-basin, this paper takes the sub-basin as the scope to construct a numerical model, and the scope of the model construction is shown in Figure 3.

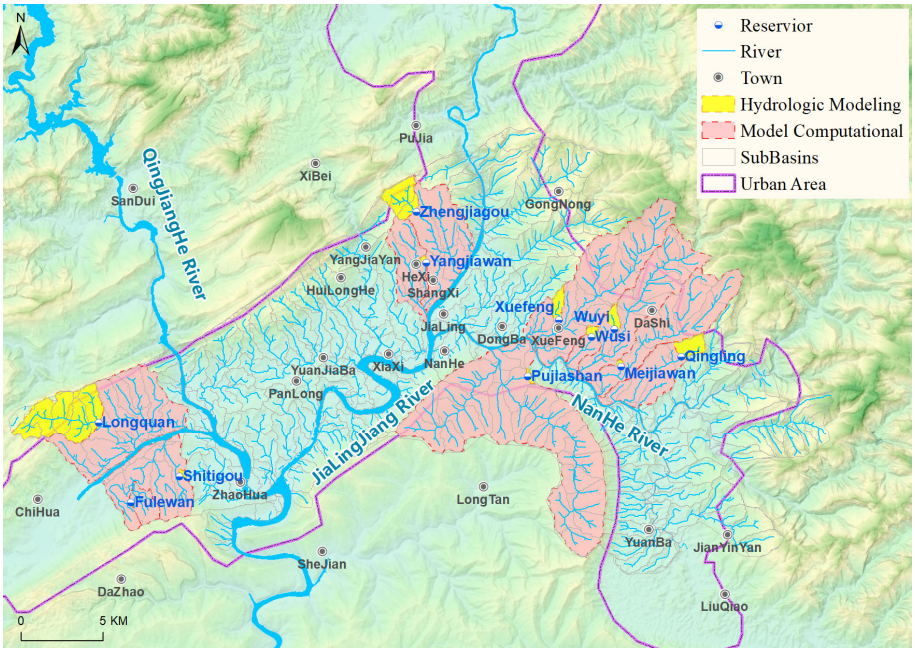


Figure 3. Scope of model construction.

2.3. Data and Methods

2.3.1. Data

The elevation data used in this study has a spatial resolution of 30 m. Cross-sectional data of flash flood gullies and river channels were obtained through manual field surveys using a depth sounder. The design rainfall data were derived from statistical analysis of nearly 30 years of precipitation records from a local hydrological station. Since there are no monitoring stations at the outlets of the mountain torrent channels within the study area, and all these torrents eventually flow into the Nanhe River (as shown in Figure 4), the design flood levels of the Nanhe River cross-sections were selected for model calibration and validation.

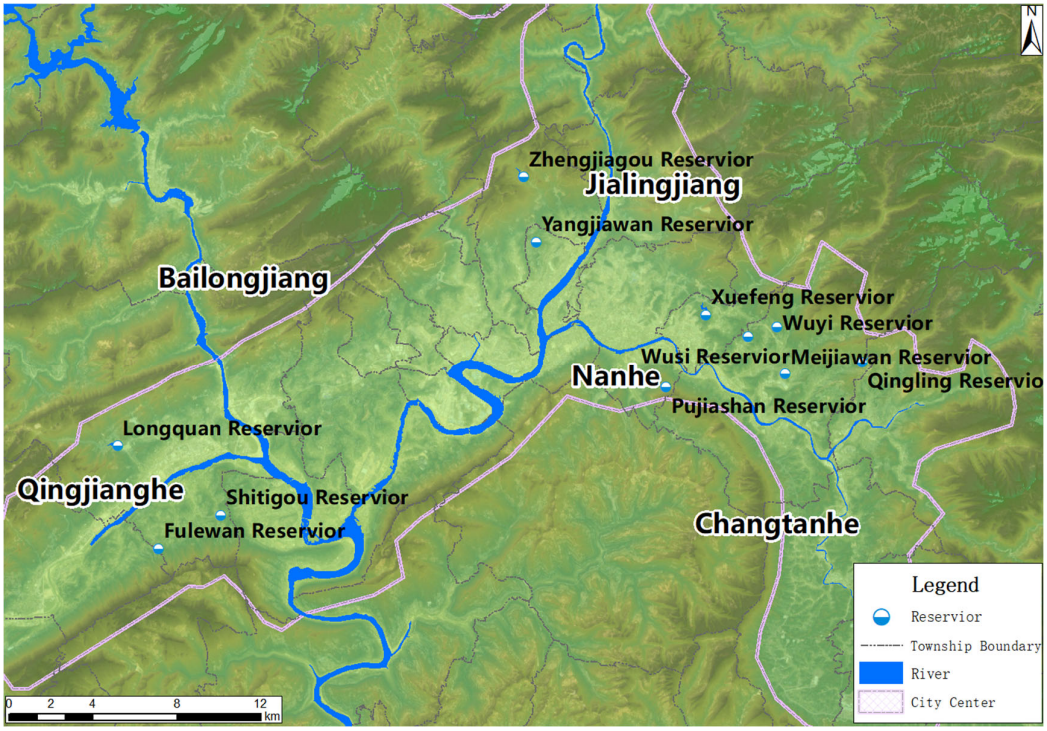


Figure 4. River distribution map.

2.3.2. Dam Failure Model

The dam breach simulation is conducted based on the actual conditions of the local reservoirs, employing an instantaneous complete failure calculation method. The specific formula is as follows [21]:

1. Calculation of Maximum Breach Flow

The estimation of breach width adopts the empirical formula developed by the Yellow River Conservancy Commission:

$$b = 0.1KW^{\frac{1}{4}}B^{\frac{1}{7}}H^{\frac{1}{2}} \quad (1)$$

where (b) represents the breach width (m), (W) denotes the total reservoir storage capacity (m^3), (H) indicates the water depth in front of the dam (m), and (K) is a parameter set to 0.65.

2. Calculation of Maximum Flow Estimates for Failure

Calculation of the maximum flow rate of a breach using the Shocklech empirical equation [22]

$$Q_{max} = (8/27) \times g^{\frac{1}{2}} \times (B/b)^{1/4} \times b \times H_0^{3/2} \quad (2)$$

where Q_{max} represents the maximum breach flow (m^3/s), H_0 denotes the upstream water depth before the dam breach (m), (B) indicates the dam length (m), and (b) signifies the breach width (m).

3. Calculation of total air release time

$$T = AW/Q_{max} \tag{3}$$

where (T) represents the total duration of the dam breach flood (s), (W) denotes the total reservoir storage capacity (m^3), and (A) is a constant set to 5.

4. Dam Breach Flood Calculation

The derivation of the instantaneous dam breach flow hydrograph typically employs the generalized typical hydrograph method, with the hydrograph shape approximated as a fourth-order parabola. The flow rapidly increases to the maximum breach flow Q_{max}, followed by a swift attenuation, forming a concave curve, and ultimately approaching the original discharge flow Q_0.

2.3.3. Hydrological Model

Based on the topography, geomorphology, and mountain torrent channel characteristics within the study area, a hydrological model is constructed for the hilly region downstream of the dam. The small watersheds in the hilly area are abstracted into distinct elements, including sub-watersheds, nodes, river segments, water sources, diversions, and depressions. The hydrological processes are disaggregated into components such as precipitation calculation, evapotranspiration calculation, runoff generation calculation, confluence calculation, and flow routing calculation. These components are used to simulate the mountain flood hydrographs under design rainfall conditions of varying frequencies.

The non-urban areas within the watershed are partitioned into independent hydrological computation units to model runoff generation, hillslope confluence, and river network confluence processes, enabling the calculation of flow hydrographs at designated control sections. The river network confluence is simulated using the lag routing method, with the computational formula expressed as follows:

$$Q(t) = CS \times Q(t-1) + (1 - CS) \times QT(t - L) \tag{4}$$

The formula is expressed as follows: $QT(t) = QS(t) + QI(t) + QG(t)$;

Where $Q(t)$ represents the river network confluence per unit area at time (m^3/s); $QT(t)$ denotes the total inflow to the river network per unit area at time (m^3/s); $QI(t)$ indicates the total interflow per unit area (m^3/s); $QG(t)$ represents the total groundwater inflow per unit area (m^3/s). This enables detailed simulation of mountain flood and dam breach risks. Here, t is the river network confluence time (s), L is the lag time (s), CS is the recession coefficient of the river network flow (dimensionless).

2.3.4. Hydrodynamic Model

Using one-dimensional and two-dimensional hydrodynamic models, this study simulates the impact of combined dam-break floods, flash floods, and intense rainfall events on downstream urban areas.

The fundamental governing equations of the one-dimensional river hydraulic model are as follows:

Continuity equations:

$$\frac{\partial A}{\partial t} + \frac{\partial Q}{\partial x} = q \tag{5}$$

Momentum equation:

$$\frac{\partial Q}{\partial t} + \frac{\partial}{\partial x}\left(\alpha \frac{Q^2}{A}\right) + gA\left(\frac{\partial y}{\partial x}\right) + gAS_f - u \cdot q = 0 \tag{6}$$

In the above equations, A is the cross-sectional flow area of the river (m^2); Q is the discharge at the cross-section (m^3/s); u is the velocity component of lateral inflow in the direction of river flow (m/s); t is time (s); x is the horizontal coordinate along the flow direction; q is the lateral inflow per unit length (m^2/s); α is the momentum correction coefficient; g is the acceleration due to gravity (m/s^2); y is the water surface elevation in the river (m); $S_f = \frac{n^2 V|V|}{R^{4/3}}$ represents the friction slope, where n is the Manning's roughness coefficient, V is the velocity (m/s), and R is the hydraulic radius (m).

The one-dimensional hydrodynamic model for the river channel employs an explicit finite difference method to discretize the governing equations in time and space. Flow is calculated using the finite difference method, while water level is solved using the finite volume method. This discretization approach has clear physical meaning, effectively handles dry bed conditions, and facilitates the incorporation of various hydraulic structures.

The basic governing equations for the two-dimensional surface water dynamics model are as follows:

Continuity equations:

$$\frac{\partial H}{\partial t} + \nabla \cdot hV + q = 0 \tag{7}$$

Momentum equation:

$$\frac{\partial V}{\partial t} + V\nabla V = -g\nabla H + v_t \nabla^2 V - c_f V + fk \times V \tag{8}$$

The momentum equation in the diffusion wave approximation, when combined with the continuity equation, offers faster computational efficiency and lower cumulative error compared to the full shallow water equations. This approach is particularly suitable for rivers with steep bed slopes. The governing equation is expressed as follows:

$$V = \frac{-(R(H))^{2/3}}{n} \frac{\nabla H}{|\nabla H|^{1/2}} \tag{9}$$

In the above equation, H is the water surface elevation (m); h is the water depth (m); V is the flow velocity (m/s); R is the hydraulic radius (m); q is the lateral inflow per unit length (m^2/s); g is the gravitational acceleration (m/s^2); v_t is the eddy viscosity in the horizontal direction (m^2/s); c_f is the bed roughness coefficient; f is the Coriolis parameter; k is the unit vector in the vertical direction; n is the Manning's roughness coefficient.

2.3.5. Model Coupling

The dam-break model, hydrological model, one-dimensional river model, and two-dimensional surface runoff-confluence model are coupled to perform simulation calculations based on the three-dimensional spatial structure and the physical mechanisms of each model. In the coupling of the hydrological and hydrodynamic models, the hydrological processes in mountainous areas are simulated first using the hydrological model, followed by the independent simulation of hydrodynamic processes. The runoff and confluence results derived from the hydrological model are used as boundary conditions for both the one-dimensional river hydrodynamic model and the two-dimensional surface hydrodynamic model.

The coupling of the one-dimensional river model and the two-dimensional surface runoff-confluence model is achieved through a time-marching method for data exchange. This coupling includes the interaction between the one-dimensional river model and the two-dimensional surface model across levees. The coupled hydrological–hydrodynamic model incorporates physical mechanisms that accurately characterize the generation and concentration of runoff caused by heavy rainfall within small watersheds in hilly regions.

During the calculation, the coupling position between the one-dimensional river channel model and the two-dimensional surface runoff hydrodynamic model is located at the embankment edge along the river channel where the river segment meets adjacent grids. Water exchange occurs when the water level in the river channel exceeds the embankment edge or when the water level in the grid exceeds the embankment edge, resulting in a flow process at the coupling position. The computational time steps for the one-dimensional river channel model and the two-dimensional surface runoff hydrodynamic model are 6 s and 0.1 s, respectively.

3. Analysis of Results

3.1. Validation

Based on the confluence characteristics of the river, the 50-year return period design flood levels at three representative cross-sections of the Nanhe River were selected for model calibration. A comparison between the model results and the design flood levels is presented in Table 1. As shown in Table 1, the differences between the simulated results and the design flood levels at the three cross-sections range from 0.17 m to 0.3 m. The model results meet the required accuracy, indicating that the modeling approach is reasonably reliable.

Table 1. Comparison of model simulation results and design water levels.

No.	River Cross-Section ID	50-Year Return Period Design Flood Levels (m)	Model Simulation Results (m)	Error (m)
1	Section-1	478.81	478.51	0.3
2	Section-2	479.04	478.87	0.17
3	Section-3	480.14	479.87	0.27

3.2. Analysis of Dam-Break Floods

The dam-break outflows from each reservoir were superimposed with the flash flood processes occurring in the downstream sections of the reservoir catchments to obtain the flow discharge at the outlet cross-sections of each watershed. Figure 5 presents the calculated peak discharges resulting from dam-break events under different rainfall return periods.

As shown in the subfigures of Figure 5, the magnitude of the dam-break flow is primarily influenced by the water level difference between the upstream and downstream sides of the breach section. The intensity of rainfall, represented by different return periods, has little impact on the peak flow generated at the breach. The hydrographs at the outlet cross-sections are characterized by high peaks and narrow shapes, and rapid rises and falls—features typical of flash flood responses in hilly terrain.

However, the flow hydrographs at the outlet cross-sections vary among the 11 reservoir catchments. For the reservoirs shown in Figure 5a–e, the outlet hydrographs display a single, prominent flood peak, while those in Figure 5f–k exhibit two distinct flood peaks. The primary reason for this difference lies in the relative location of the reservoir within the catchment and its distance from the outlet cross-section.

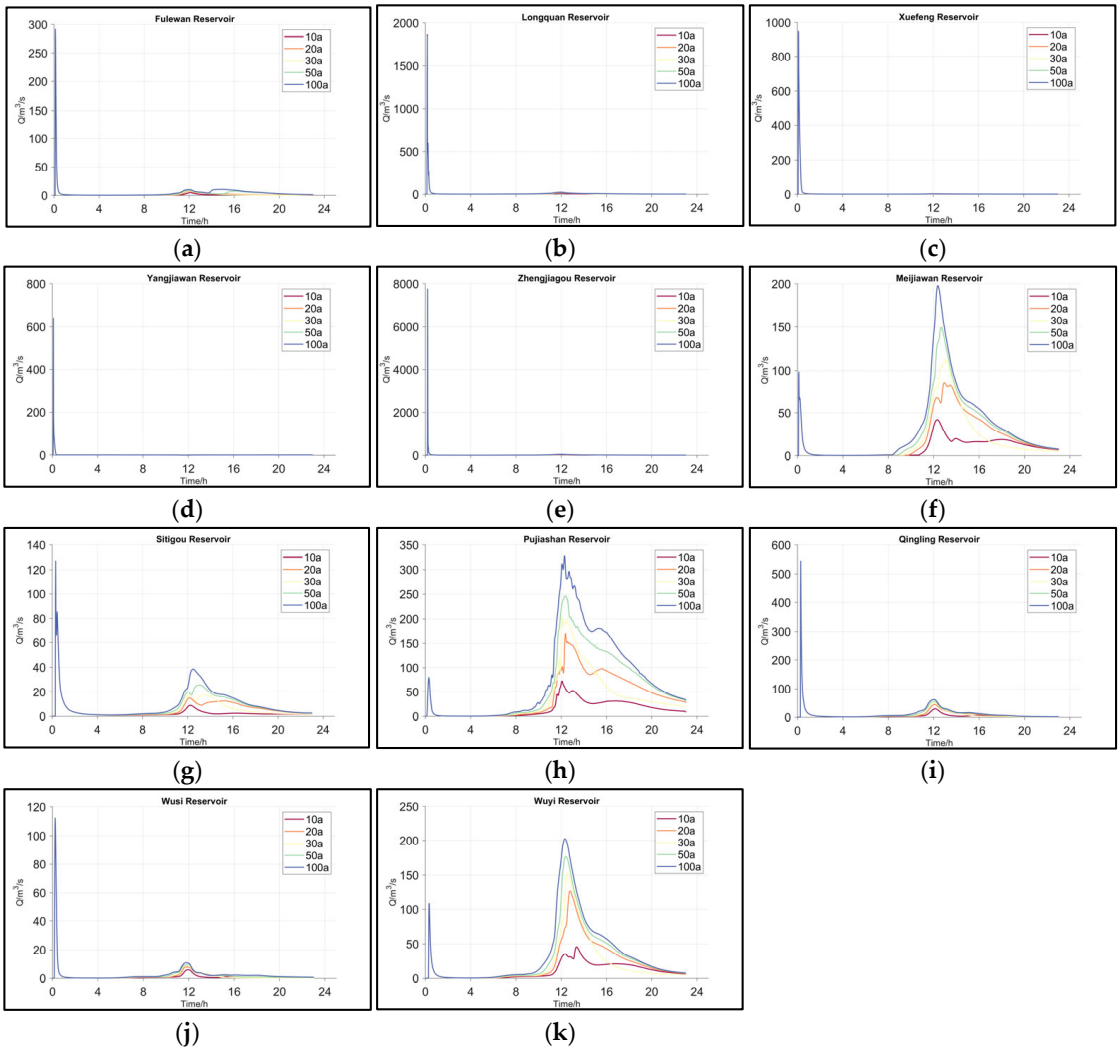


Figure 5. Flow processes at the outlet section of the sub-basin. (**a**) Fulewan Reservoir; (**b**) Longquan Reservoir; (**c**) Xuefeng Reservoir; (**d**) Yangjiawan Reservoir; (**e**) Zhengjiagou Reservoir; (**f**) Meijiawan Reservoir; (**g**) Sitigou Reservoir; (**h**) Pujiashan Reservoir; (**i**) Qingling Reservoir; (**j**) Wusi Reservoir; (**k**) Wuyi Reservoir.

For the reservoirs in Figure 5a–e, the small reservoirs are located close to the outlet cross-sections, and the outlet floods are mainly composed of dam-break flows. In contrast, for the reservoirs in Figure 5f–k, the reservoirs are situated farther from the outlet, with larger downstream contributing areas. In these cases, the first flood peak at the outlet results from the dam-break flood, while the second peak is primarily caused by rainfall-induced flash flooding in the downstream area. A comparison of upstream and downstream catchment areas for reservoirs exhibiting double-peaked hydrographs at the outlet cross-sections is provided in Table 2.

As shown in Table 2, for reservoirs where double-peaked flood hydrographs occur at the outlet cross-sections, the average contributing area of the reservoir accounts for only 2.6% of the downstream catchment area—significantly smaller than the area below the dam. Following a dam-break event, the resulting flood peak propagates rapidly downstream, while rainfall continues to generate runoff in the downstream region. Compared with the sharp, narrow hydrograph of the dam-break flood, the flood wave generated by rainfall in the downstream area is relatively broader and flatter.

Table 2. Comparison table of upstream and downstream areas of the reservoir during the double peak flood process at the exit section.

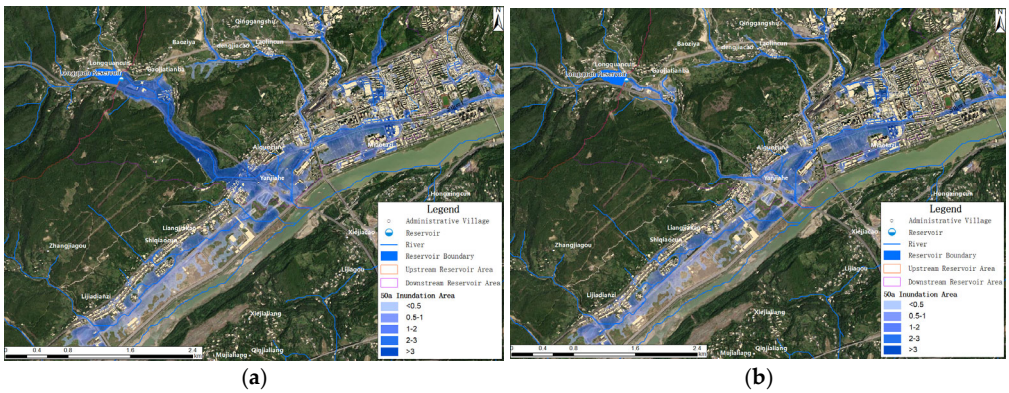
No.	Reservoir Name	Total Storage Capacity (Million m^3)	Upstream Catchment Area (km^2)	Downstream Catchment Area (km^2)	Area Ration (%)
1	Sitigou Reservoir	26.4	0.28	18.61	1.5
2	Pujiashan Reservoir	10.12	0.177	61.87	0.29
3	Wuyi Reservoir	10.66	0.8	22.04	3.63
4	Meijiawan Reservoir	10.83	0.15	12.32	1.22
5	Qingling Reservoir	37.02	1.7	28.63	5.94
6	Wusi Reservoir	15.47	0.38	12.66	3
		Average Value			2.60

For reservoirs with large downstream contributing areas, the peak discharge and total flood volume generated by rainfall-induced flash floods may exceed those produced by the dam-break event itself.

The catchment area of the Pujia Mountain Reservoir is 61.87 km^2. Due to the considerable distance between the dam and the downstream outlet section, as well as the large contributing area, two distinct flood peaks were observed at the downstream outlet section. The first peak was sharp and narrow, resulting from the dam breach, and formed within just one hour following the sudden failure of the Pujia Mountain Reservoir. The second peak occurred later and was primarily caused by rainfall within the watershed, completing its evolution within 2 to 3 h.

3.3. Analysis of Inundation Results

Due to space limitations, this study focuses on the Longquan Reservoir catchment under a 50a return period rainfall event as a representative case. Figure 6 illustrates the inundation extent, while Figure 7 shows the maximum flow velocity distribution. As seen in Figure 6, when a dam breach occurs at the Longquan Reservoir, the inundated area increases significantly compared to the non-breach scenario. In both cases, most of the urban area experiences inundation depths of less than 0.5 m, and the difference in inundated areas with depths less than 1 m is relatively small. However, for inundation depths exceeding 1 m, the inundated area in the dam breach scenario is significantly larger than in the no-breach case. When no breach occurs, the inundation depth in the downstream urban area is mainly concentrated below 0.5 m; in contrast, with a dam breach, the area with inundation depths exceeding 1 m accumulates to more than 3 km^2.



(**a**) (**b**)

Figure 6. Comparison of the inundation area of Longquan Reservoir with and without dam failure. (**a**) Scope of 50a return period rainfall inundation. (**b**) Scope of 50a return period rainfall in case of dam break.

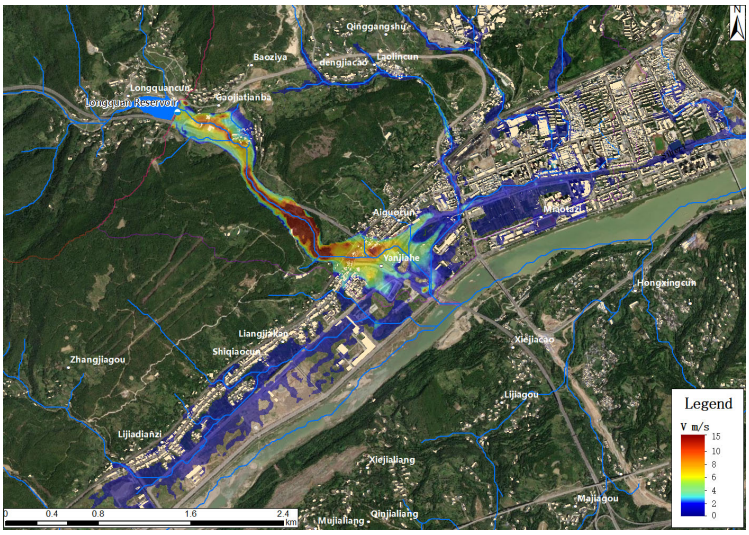


Figure 7. Maximum flow velocity distribution map.

As shown in Figure 7, in the event of a dam breach, the flood flow velocity becomes extremely high, with maximum velocities exceeding 15 m/s. Within the downstream urban area, the average flow velocity reaches approximately 10 m/s, which could pose severe impacts on the city.

A comparison between the inundated areas resulting from the combined effects of dam breach and rainfall, and those caused by rainfall alone, is presented in Table 3. As shown in Table 3, the inundated area increases with the rising frequency of heavy rainfall events; however, the increase is relatively limited. This is primarily due to the geomorphological characteristics of mountainous cities, where steep gullies and incised river valleys typically exhibit "U"- or "V"-shaped cross-sections. Under rainfall events of different return periods, the extent of floodplain overflow along both sides of the channels does not vary significantly.

Table 3. Comparison of inundation area of reservoir breach and no breach urban areas under different return period rainfall conditions.

Rainfall Return Period	Maximum Depth of Inundation (m)	<0.5	0.5–1	1–2	2–3
10a	Area Inundated by Dam Failure (km^2)	4.22	1.94	2.01	1.07
	Area of Inundation without Dam Failure (km^2)	3.84	1.81	1.67	0.33
20a	Area Inundated by Dam Failure (km^2)	4.28	2.13	2.31	1.29
	Area of Inundation without Dam Failure (km^2)	3.88	1.99	2.15	0.53
30a	Area Inundated by Dam Failure (km^2)	4.3	2.17	2.41	1.31
	Area of Inundation without Dam Failure (km^2)	3.88	2.03	2.27	0.59
50a	Area Inundated by Dam Failure (km^2)	4.31	2.21	2.54	1.38
	Area of Inundation without Dam Failure (km^2)	3.88	2.08	2.4	0.67
100a	Area Inundated by Dam Failure (km^2)	4.31	2.24	2.66	1.43
	Area of Inundation without Dam Failure (km^2)	3.85	2.14	2.51	0.76

4. Conclusions

This paper analyzes the compound risk of dam-break floods and flash floods in mountainous valley cities by constructing a dam-break model, a hydrological model, and a hydrodynamic model. Based on the analysis, the following conclusions are drawn:

1. In upstream areas of mountainous cities, if a small reservoir experiences a dam-break, the resulting flood peak is characterized by a high magnitude and rapid rise and fall, typically completing its course within one hour. In contrast, flash floods induced

by downstream rainfall generally evolve over a period of 2–3 h. For reservoirs with relatively large downstream catchment areas, rainfall-induced flows can be substantial. When heavy rainfall occurs in the hilly upstream region of such reservoirs, the dam-break flood and the flash flood caused by downstream rainfall may result in a two-stage impact on the city. Dam failure of this type of reservoir poses a more severe threat and thus warrants particular attention for risk prevention.

2. The risk of reservoir dam-break is closely related to the water level difference between the upstream and downstream sides of the dam. A greater water level difference results in higher hydraulic pressure on the dam structure, significantly increasing the likelihood of failure. Therefore, prior to the onset of extreme rainfall events, it is essential to implement pre-release operations in accordance with reservoir regulation plans, aiming to lower the upstream water level in advance and thereby minimize the risk of dam-break and its potential impacts on downstream areas.
3. With the increasing frequency of extreme rainfall events, the inundation area in urban regions expands accordingly; however, the extent of this increase remains limited. This is primarily due to the geomorphological characteristics of mountainous cities, where flash flood channels and river valleys are deeply incised, typically exhibiting "U"- or "V"-shaped cross-sections. Under rainfall events of varying return periods, the extent of overbank flooding along these channels changes minimally. In mountainous urban areas, the primary hazard arises from the high-velocity flow. Flash floods are characterized by large discharges and high flow velocities, with peak velocities reaching up to 15 m/s, posing significant threats to downstream urban areas.
4. Mountainous valley cities exhibit distinct topographical characteristics that should be strategically leveraged to optimize flood risk management. Effective regulation of upstream reservoirs can significantly reduce the risk of dam failure. Additionally, implementing flood diversion measures at the mountain front can redirect flash floods to bypass the main urban area and discharge downstream. Enhancing overland flow management on slopes can prevent the convergence of flood peaks, thereby improving the city's capacity for energy dissipation, flow attenuation, and peak reduction. A combination of structural and non-structural measures should be adopted to comprehensively strengthen Guangyuan's flood resilience. To enhance the practical value of this research, it is recommended to further explore how these measures can be implemented in Guangyuan City, incorporating considerations of cost and feasibility constraints.
5. This study takes Guangyuan City as an example. However, different mountainous cities have distinct characteristics. Therefore, in modeling, it is necessary to consider the geographical and climatic features of each city and select appropriate models accordingly. For instance, in coastal mountainous cities, the impact of typhoon-induced rainfall must be considered, as it is typically intense and long-lasting. This requires adjusting parameters such as rainfall duration and intensity. In contrast, inland mountainous cities often have steeper slopes and longer main channels in mountain gullies, necessitating adjustments to surface condition parameters in the flood models. Thus, model modifications should be made based on the topography, hydrology, climate, and engineering features of the target city. By developing a similarity assessment system or incorporating regional parameter adjustment modules, the model's applicability and accuracy can be enhanced. Coastal, plateau, and arid mountainous cities each have specific risk characteristics and mountain flood formation mechanisms.

Author Contributions: Y.L. (Yesen Liu), and Q.Y. collected and processed the data, Y.L. (Yuanyuan Liu), and S.L. and Q.Y. proposed the model and analyzed the results, and Y.L. (Yuanyuan Liu) and Y.L. (Yesen Liu) wrote the manuscript. All authors have read and agreed to the published version of the manuscript.

Funding: This work is supported by National Natural Science Foundation of China (52394235), the National Natural Science Foundation of China (No. U2340225), MWR Talented Expert Program (No. JHQB202221).

Institutional Review Board Statement: Not applicable.

Informed Consent Statement: Not applicable.

Data Availability Statement: The participants of this study did not agree for their data to be shared publicly, so supporting data is not available.

Conflicts of Interest: The authors declare no conflicts of interest.

References

1. Huang, G.Y. Ecological thinking over spatial structure of hilly city. *City Plan. Rev.* **2005**, *29*, 57–63.
2. Tayfur, G.; Guney, M.S. A physical model to study dam failure flood propagation. *Water Util. J.* **2013**, *6*, 19–27.
3. Haltas, I.; Tayfur, G.; Elci, S. Two-dimensional numerical modeling of flood wave propagation in an urban area due to Ürkmez dam-break, İzmir, Turkey. *Nat. Hazards* **2016**, *81*, 2103–2119. [CrossRef]
4. Jeong, W.; Yoon, J.S.; Cho, Y.S. Numerical study on effects of building groups on dam-break flow in urban areas. *J. Hydro-Environ. Res.* **2012**, *6*, 91–99. [CrossRef]
5. Cheng, X.; Liu, C.; Li, C.; Yu, Q.; Li, N. Evolution characteristics of flood risk under changing environment and strategy of urban resilience improvement. *J. Hydraul. Eng.* **2022**, *53*, 757–768+778.
6. Doerge, B.C. Failure Modes of Cohesive Soil Subject To Flow: A Dam Failure Case Study. In Proceedings of the Association of State Dam Safety Officials Annual Conference, Denver, CO, USA, 16–20 September 2012; Volume 2.
7. Mehta, A.M.; Weeks, C.S.; Tyquin, E. Towards preparedness for dam failure: An evidence base for risk communication for downstream communities. *Int. J. Disaster Risk Reduct.* **2020**, *50*, 101820. [CrossRef]
8. Liu, Y.; Liu, Y.; Liu, Z.; Lin, Y.; Chen, Y.; Li, K.; Liu, Y. Preliminary discussion on flood control standard and flood control engineering measures in mountainous cities. *J. China Inst. Water Resour. Hydropower Res.* **2023**, *21*, 341–349.
9. Froese, C.R.; Moreno, F. Structure and components for the emergency response and warning system on Turtle Mountain, Alberta, Canada. *Nat. Hazards* **2014**, *70*, 1680–1712. [CrossRef]
10. Reed, S.; Schaake, J.; Zhang, Z. A distributed hydrologic model and threshold frequency-based method for flash flood forecasting at ungauged locations. *J. Hydrol.* **2007**, *337*, 402–420. [CrossRef]
11. Elbastawesy, M.; White, K.; Nasr, A. Integration of remote sensing and GIS for modeling flash floods in Wadi Hudain catchment, Egypt. *Hydrol. Process.* **2009**, *23*, 1359–1368. [CrossRef]
12. Santos, J.G. GIS-based hazard and risk maps of the Douro River basin (north-eastern Portugal). *Geomat. Nat. Hazards Risk* **2015**, *6*, 90–114. [CrossRef]
13. Dutta, D.; Alam, J.; Umeda, K.; Hayashi, M.; Hironaka, S. A two-dimensional hydrodynamic model for flood inundation simulation: A case study in the lower Mekong River Basinji. *Hydrol. Process.* **2007**, *21*, 1223–1237. [CrossRef]
14. Glotov, V.E.; Chlachula, J.; Glotova, L.P.; Little, E. Causes and environmental impact of the gold-tailings dam failure at Karamken, the Russian Far East. *Eng. Geol.* **2018**, *245*, 236–247. [CrossRef]
15. Youssef, A.M.; Pradhan, B.; Hassan, A.M. Flash flood risk estimation along the st. Katherine road, southern sinai, Egypt using GIS based morphometry and satellite imagery. *Environ. Earth Sci.* **2011**, *62*, 611–623. [CrossRef]
16. Ballesteros-Canovas, J.A.; Czaika, B.; Janecka, K.; Lempa, M.; Kaczka, R.J.; Stoffel, M. Flash floods in the Tatra Mountain streams: Frequency and triggers. *Sci. Total Environ.* **2015**, *511*, 639–648. [CrossRef] [PubMed]
17. Cai, Z.; Chu, S.Z.; Liu, H.W.; Min, X. Application research of computational fluid dynamics model in flood routing of urban underground three-dimensional disaster bearing bodies. In Proceedings of the 2024 (Third) Symposium on Urban Water Conservancy and Flood Prevention and Control, Hangzhou, China, 13 December 2024; Nanjing Institute of Water Resources Science: Nanjing, China, 2024. [CrossRef]
18. Kritikos, T.; Davies, T. Assessment of rainfall-generated shallow landslide/debris-flow susceptibility and runout using a GIS-based approach: Application to western Southern Alps of New Zealand. *Landslides* **2015**, *12*, 1051–1075. [CrossRef]
19. He, X.; Chen, C.; Liu, Y.; Chu, Y. Inundation Analysis Method for Urban Mountainous Areas Based on Soil Conservation Service Curve Number (SCS-CN) Model Using Remote Sensing Data. *Sens. Mater.* **2020**, *32*, 3813–3822. [CrossRef]

20. Ouyang, C.; He, S.; Xu, Q.; Luo, Y.; Zhang, W. A MacCormack-TVD finite difference method to simulate the mass flow in mountain ous terrain with variable computational domain. *Comput. Geosci.* **2013**, *52*, 1–10. [CrossRef]
21. Xie, R.-Z. *Dam Hydraulics*; Shandong Science and Technology Press: Jinan, China, 1996.
22. Dai, R.Y.; Wang, Q. Research on the maximum discharge of dam-breaking. *J. Hydraul. Eng.* **1983**, *2*, 15–23.

Disclaimer/Publisher's Note: The statements, opinions and data contained in all publications are solely those of the individual author(s) and contributor(s) and not of MDPI and/or the editor(s). MDPI and/or the editor(s) disclaim responsibility for any injury to people or property resulting from any ideas, methods, instructions or products referred to in the content.